

# Chapter 61

## Underground Flow Section Modification Below the New M3 Flon Metro Station in Lausanne



**Leona Repnik, Samuel Vorlet, Mona Seyfeddine, Azin Amini,  
Romain Dubuis, Giovanni De Cesare, Pierre Bourqui,  
and Pierre-Adil Abdelmoula**

**Abstract** Rapid urbanization is increasing the demand for public transport in Switzerland's major cities. The new m3 metro line in Lausanne is planned to circulate by 2030. Its construction will require a modification of the underground flow section of the Flon River vaulting at the Flon metro station. The Flon River drains a natural watershed, as well as the combined sewage network of the city of Lausanne. Two prior modifications of the vaulting geometry at the Flon station were carried out to accommodate the infrastructure of the m2 and LEB metro lines. The research aim was to assess the proposed vaulting geometry underneath the m3 by means of a hybrid hydraulic modelling approach combining a numerical and physical model in order to evaluate the new capacity limit of the system. A design discharge of  $90 \text{ m}^3/\text{s}$  was defined, corresponding to a 100-year return period. A 3D numerical model at prototype scale was developed in the commercial software packages ANSYS Fluent

---

L. Repnik (✉) · S. Vorlet · M. Seyfeddine · A. Amini · R. Dubuis · G. De Cesare  
Hydraulic Constructions Platform (PL-LCH), École Polytechnique Fédérale de Lausanne (EPFL),  
Station 18, 1015 Lausanne, Switzerland  
e-mail: [leona.repnik@alumni.epfl.ch](mailto:leona.repnik@alumni.epfl.ch)

S. Vorlet  
e-mail: [samuel.vorlet@epfl.ch](mailto:samuel.vorlet@epfl.ch)

M. Seyfeddine  
e-mail: [mona.seyfeddine@epfl.ch](mailto:mona.seyfeddine@epfl.ch)

A. Amini  
e-mail: [azin.amini@epfl.ch](mailto:azin.amini@epfl.ch)

R. Dubuis  
e-mail: [romain.dubuis@epfl.ch](mailto:romain.dubuis@epfl.ch)

G. De Cesare  
e-mail: [giovanni.decesare@epfl.ch](mailto:giovanni.decesare@epfl.ch)

P. Bourqui · P.-A. Abdelmoula  
Stucky SA, Rue du Lac 33, BP 80, 1020 Renens VD, Switzerland  
e-mail: [pierre.bourqui@stucky.ch](mailto:pierre.bourqui@stucky.ch)

P.-A. Abdelmoula  
e-mail: [pierre-adil.abdelmoula@stucky.ch](mailto:pierre-adil.abdelmoula@stucky.ch)

and Flow-3D to simulate a multiphase flow. The physical model was built at a reduced scale of 1:20 based on Froude similarity. Taking into account the precision of the measurements on the physical model and the accuracy of the numerical results, they are all within the assumed limitations. Regarding the engineering project, the results indicate that the design discharge cannot be maintained under free surface flow conditions with the proposed vaulting geometry. The main limitation for the validation of the results is the lack of in-situ stage-discharge data.

**Keywords** ANSYS fluent · Flow-3D · Numerical modelling · Physical modelling · Urban underground flow

## 61.1 Introduction

As urban areas are growing rapidly, the demand for public transport in Switzerland's major cities is increasing [1–3]. As part of the expansion of the public transport network in the agglomeration of Lausanne, a third metro line (hereafter referred to as “m3”) will be put in place by 2030. One of the stops will be the Flon metro station, which already hosts the m1, m2 and LEB metro lines. The expansion of the Flon metro station for the new m3 will require a modification of the historical vaulting through which the Flon River flows [4]. This will lead to a change in the underground hydraulic section of the Flon River. Several geometries have been proposed for the modified stretch of the m3 station. In the context of the m3 engineering works, this research aims to assess the proposed vaulting geometry by means of a hybrid hydraulic modelling approach in order to evaluate the new capacity limit of the system.

Traditionally, two distinct methods for studying and analyzing hydraulic phenomena existed: numerical and physical models [5]. With the rapid development of numerical methods, the use of physical models has declined, given the costs of such installations [5]. The use of CFD tools for numerical modelling have shown to add value to the design and analysis of urban drainage systems, especially in the case of combined sewer overflows [6]. Despite numerical methods becoming more frequently used for hydraulic problems, a physical model allows to maintain a physical reality of the studied phenomenon, better observation of the flow and improved visualization for communicating results [5].

A hybrid modelling approach, combining CFD tools and a physical model, has been less commonly used. Nevertheless, some studies of hydraulic problems, including in the context of urban drainage engineering, exist. Rubinato et al. [7] compared water levels between a 2D numerical model and a physical model to determine the capacity of a circular sewer inlet under steady state hydraulic conditions. Lopes et al. [8] used a full-scale (1:1) physical model to validate a 3D numerical OpenFOAM model of a gully to improve urban drainage efficiency during flood events. Similarly, Djordjevic et al. [9] used a comparison between a full-scale physical model and a 3D numerical model to study the interaction between gullies and below ground drainage systems. However, most research has compared a numerical

model to a full-scale experimental set-up and has been focused on smaller features of sewer systems, such as manholes and gullies [10]. A hybrid approach combining a 3D numerical model and a reduced scale physical model for the study of large-scale features in an urban drainage network, such as a river vaulting, has not been found in the literature. Furthermore, making use of such a hybrid approach to facilitate the decision-making process also provides a research gap that will be addressed in this study.

## 61.2 Background

### 61.2.1 Study Location

The study is carried out on the vaulting of the Flon River at the Flon metro station in the city of Lausanne, Switzerland. The Flon River drains a watershed of 23 km<sup>2</sup>, which is natural in the upstream portion and drains the combined sewage network of the city on the inferior portion. Before flowing through the vaulting as part of the sewage network, part of the Flon River discharge is diverted into the neighbouring Vuachère River, with the goal of reducing clear water discharge to the wastewater treatment plant. The Flon River eventually reaches the Vidy wastewater treatment plant, after which the water is released into Lake Geneva. The landcover of the catchment is dominated by urban area. The total length of the river from its source to Lake Geneva is 11.5 km and the mean annual discharge is 1 m<sup>3</sup>/s [11].

Historically, the Flon River played an important role in allowing the expansion of human settlements since the Middle Age, and later on, promoting the economic development of the city of Lausanne [11]. The river was not only used to harness its energy through the water mills, but it was also important for evacuating solid and liquid waste from the city [11]. However, strong development of industrial activities on the riverbanks and rapid urbanization led to several consequences, including pandemic outbreaks caused by the wastewater and disastrous flood events [12]. Between the nineteenth and twentieth century, the City of Lausanne decided to undertake construction works to fill the Flon valley and place the river underground in a vaulting [11].

The Flon vaulting has been subject to several modifications due to historical engineering works for the construction of the LEB and m2 metro lines. These works took place at the Flon metro station and have changed the hydraulic section of the river. Most importantly, these works have led to many transition zones of the vaulting geometry, which have created complex flow conditions of the Flon River. In addition, the study site is located at a bend, which creates further complexities. The planned construction works for the m3 will take place immediately upstream of the m2 stretch (Fig. 61.1).

A 1D analysis of the Flon River vaulting in the context of the m3 engineering works was carried out by Bourqui [4]. Several potential geometries were tested for



**Fig. 61.1** Modifications of the Flon River vaulting at the Flon station. The historical works included modifications for the LEB and m2 metro lines, which are downstream of the planned m3. The historical vaulting remains upstream of the m3 and downstream of the LEB. The planned m3 tracks and the m3 Flon station (red lines) and the flow direction (blue arrow) are shown. Taken from Bourqui [4]

the m3 stretch, characterized by a reduced ceiling height and an enlargement of the cross-section width (Fig. 61.2). A maximum ceiling height was defined at an altitude of 471.3 m a.s.l. (corresponding to a maximum cross-sectional height of 2.5 m) and the most favourable geometry is characterized by a maximum width of 8.16 m [4]. This geometry will be tested in the numerical and physical models to ensure that the capacity is maintained for the design discharge of 90 m<sup>3</sup>/s, corresponding to a 100-year return period. Specifically, the following three hydraulic criteria must be attained:

1. The free surface filling ratio must not exceed 85% of available maximum height
2. A minimum safety margin (freeboard) of 60 cm must be maintained in case of floating debris
3. The flow must not touch the ceiling locally



**Fig. 61.2** Photograph of the inside of the Flon River vaulting looking downstream. The photo was taken at the location where the historical vaulting (characterized by the rounded ceiling, locally reconstructed with precast concrete elements as transition from the original brick section) will be replaced for the new m3. The reduced ceiling height in the background represents the modified section for the existing m2. *Picture Pierre Bourqui*

## 61.2.2 Theoretical Background

### 61.2.2.1 Flow Classification

Open channel flow, also known as free surface flow, is characterized by having a free water surface exposed to the ambient atmosphere, in contrast to closed conduit or pressurized flow [13, 14]. Open channel flow is classed as steady if flow parameters (e.g. mean cross-sectional depth, velocity, discharge, surface roughness, slope) do not change with time, in contrast to unsteady flow [13–15]. Uniform flow occurs when the flow parameters remain constant in the flow direction and thus do not change over space [14, 15]. This requires a uniform bed slope, roughness and channel geometry (cross-section) in streamwise direction [15, 16]. Thus, the slope of the water level (hydraulic grade line), the friction slope (energy grade line) and the physical slope of the channel bottom are parallel [13, 14]. The Manning–Strickler equation, most commonly used to solve open channel flow problems [17], is given by:

$$V = \frac{1}{n} R^{2/3} J^{1/2} \quad (61.1)$$

with  $V$  the mean flow velocity,  $n$  Manning's coefficient,  $R$  the hydraulic radius and  $J$  the energy slope. Given that open channel flow is characterized by a free surface,

the driving force is gravity [15]. Therefore, the most important force ratio for open channel flow is the dimensionless Froude number:

$$Fr = \left( \frac{\textit{inertial force}}{\textit{gravitational force}} \right)^{\frac{1}{2}} = \frac{V}{\sqrt{gL}} \quad (61.2)$$

with  $g$  the gravitational acceleration and  $L$  the characteristic length scale, commonly given by the mean water depth [15]. When  $Fr = 1$  the flow is termed critical and is characterized by unstable flow conditions creating undular waves, when  $Fr > 1$  the flow is supercritical with high velocities and small water depths and when  $Fr < 1$  the flow is subcritical with low velocities and high water depths [16].

The concept of specific energy relative to the channel bottom was first introduced by Bakhmeteff et al. [18] and can be used to define critical water depth. It is given by the sum of the velocity and pressure heads:

$$E = \frac{V^2}{2g} + y = \frac{Q^2}{2gA^2} + y \quad (61.3)$$

with  $Q$  the discharge and  $A$  the cross-sectional area. The specific energy diagram provides the variation in specific energy with water depth for a constant discharge [15, 16]. The diagram indicates that a given discharge can be passed through the channel at two different flow depths, while having the same specific energy. These two depths are termed alternate depths and represent subcritical (upper limb) or supercritical flow (lower limb) [14, 16]. When the specific energy reaches its minimum, the critical flow condition is attained ( $Fr = 1$ ), known as the critical depth ( $h_{crit}$ ).

### 61.2.2.2 Physical Modelling Scale Effects

Scale effects refer to differences in physical behaviour occurring between a real-world prototype and its down-scaled physical model, potentially causing misleading predictions [19]. Scale effects are caused by non-identical force ratios between a physical hydraulic model and the prototype observations, which results in deviations between the two [20]. The only scale at which all factors are consistent and there are no scale effects is 1:1 ( $\lambda = 1$ ) [20]. As  $\lambda$  increases, the modelled force ratios diverge from the prototype ratios and thus, the scale effects become larger [20].

Model-prototype similarities include geometric, kinematic and dynamic similarities [20–22]. These three conditions must be met in order to have complete mechanical similarity between a prototype and its model, and therefore no scale effects. Geometric similarity (length-scale equivalence) means the length dimensions can be scaled by a constant scale factor [23]. Kinematic similarity (time-scale equivalence) refers to the similarity in the motion of model and prototype particles, requiring

constant ratios of acceleration, discharge, time and velocity in the model and prototype [20, 22]. Dynamic similarity (force-scale equivalence) refers to constant force ratios and it is the most restrictive similarity condition [20].

Since it is impossible to maintain all relevant force ratios constant, the force ratio that dominates the physical phenomenon being investigated should be selected. For most hydraulic studies involving free surface flows, Froude similarity is used [24]. However, scale effects may arise due to the Reynolds number. A sufficiently large Reynolds number ( $Re > 10^5$ ) implies that scale effects on the flow will be minimal [21, 22]

### 61.3 Methods

#### 61.3.1 Numerical Method

##### 61.3.1.1 Fluent

A 3D numerical model at prototype scale was created in ANSYS 2019 R1. The research methodology is presented in Fig. 61.3. The geometry was imported into ANSYS SpaceClaim from an Inventor drawing and covers a total length of 152.7 m with a slope of 1.03%. After simplification of the faces, a tetrahedral mesh was created using the ANSYS meshing tool, with a refinement in the form of an inflation along all walls. A sensitivity analysis was conducted with four mesh configurations

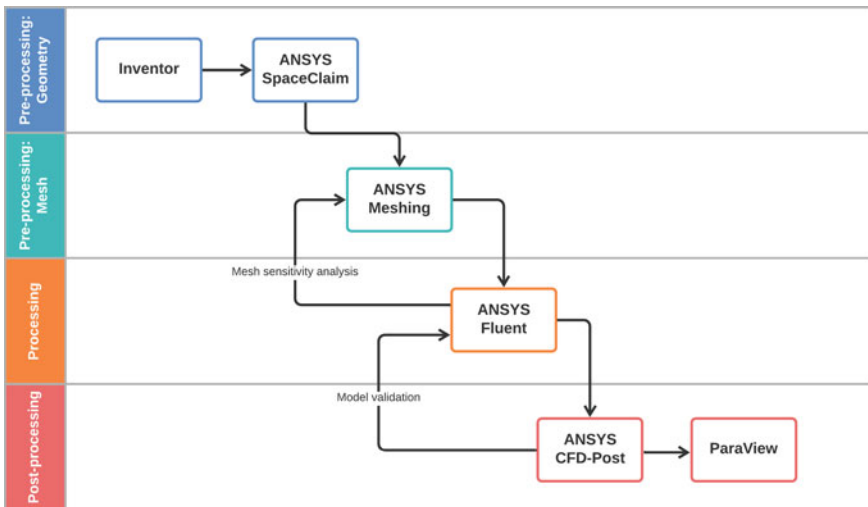
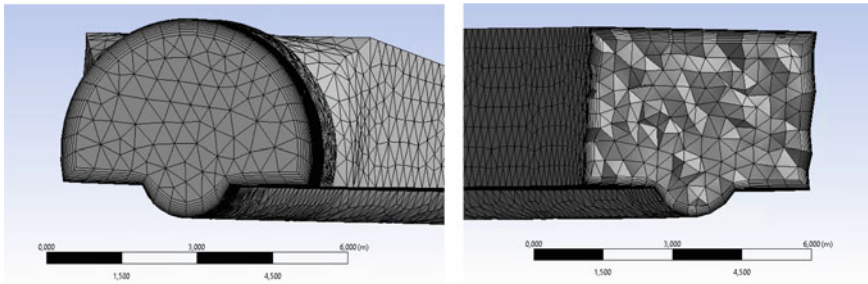


Fig. 61.3 Research methodology flow chart showing the pre-processing (blue and turquoise), processing (orange) and post-processing (red) steps



**Fig. 61.4** Selected mesh with a maximum element size 0.4 m. The historical vault (left) and rectangular LEB cross-section (right) are shown

of varying element sizes (0.2, 0.3, 0.4 and 0.5 m) to obtain representative results. Following this analysis, the mesh with an element size of 0.4 m was selected, which contains 518,964 elements and 188,330 nodes (Fig. 61.4).

The mesh was imported into ANSYS Fluent, which solves the Navier–Stokes equations using the finite volume method. For the boundary conditions, the inlet was set as a velocity inlet with a velocity of zero for the air phase and a transient velocity input with a uniform velocity distribution across the cross-section for the water phase. The transient velocity input allowed for a progressive increase in velocity, resp. discharge during the simulation. Specifically, three velocities were defined: the mean annual discharge of the Flon River ( $1 \text{ m}^3/\text{s}$ ), the velocity corresponding to half the simulated discharge and the velocity corresponding to the discharge being simulated. For each velocity, the corresponding water level was defined based on a theoretical Strickler analysis. The outlet was defined as a pressure outlet with a gauge pressure representing atmospheric pressure. The backflow of water at the outlet was prevented by selecting the volume fraction specification to *backflow volume fraction* with a value of zero. Walls were assigned a no-slip shear condition. An equivalent sand-grain roughness, representing only the roughness of the surface, was defined according to the type of construction material of the vaulting ( $k_s = 5 \text{ mm}$  for the historical vaulting and the base of the entire geometry;  $k_s = 1 \text{ mm}$  for the newer geometries: m2, m3 and LEB stretches). Hybrid initialization was computed from the velocity inlet.

A pressure-based transient solver was used. To simulate multiphase flow, the volume of fluid (VOF) method, first developed by Hirt and Nichols [25], was selected for modelling the interface between the liquid (water) and gas (air) phases. For this, the volume fraction  $\alpha$  is computed for each cell ( $\alpha = 1$  indicates the cell is filled entirely with water,  $\alpha = 0$  indicates the cell is filled with air and  $0 < \alpha < 1$  indicates the presence of a liquid–air interface) [26]. The RNG  $k\text{-}\epsilon$  turbulence model was selected. The RNG option, first developed by Yakhot and Orszag [27], is more accurate than the standard  $k\text{-}\epsilon$  model and allows application to a wider range of flows [28]. A summary of the numerical model setup is given in Table 61.1. The simulation time was set to 180 s to achieve steady state conditions. A variable time stepping method



**Table 61.1** Numerical setup of the 3D Fluent model

Property	Setting
Solver	Pressure-based transient
Viscous model	k-ε (RNG option)
Pressure-velocity coupling scheme	Simple
Spatial discretization: Gradient	Least squares cell based
Spatial discretization: Pressure	Body force weighted
Spatial discretization: Momentum	Second order upwind
Spatial discretization: Volume fraction	Compressive
Spatial discretization: Turbulent Kinetic Energy	Second order upwind
Spatial discretization: Turbulent Dissipation Rate	Second order upwind
Transient formulation	First order implicit

was defined, with a global Courant number of 1, a minimum time step size of 0.05 s and a maximum time step size of 10 s. Convergence was monitored through basic convergence criteria.

Seven discharge scenarios were tested:  $Q = 20, 30, 40, 60, 70, 80$  and  $90 \text{ m}^3/\text{s}$ . The latter is the design discharge, corresponding to a return period of 100 years. Twelve measurement locations were defined, representing changes in hydraulic section (Fig. 61.5). The model was validated at measurement location 2 by comparison to a theoretical Strickler analysis and 1D HEC-RAS model. In addition, a comparison to the experimental data from the physical model was carried out, as done by [29]. Visualization was done in ParaView 5.8.0.

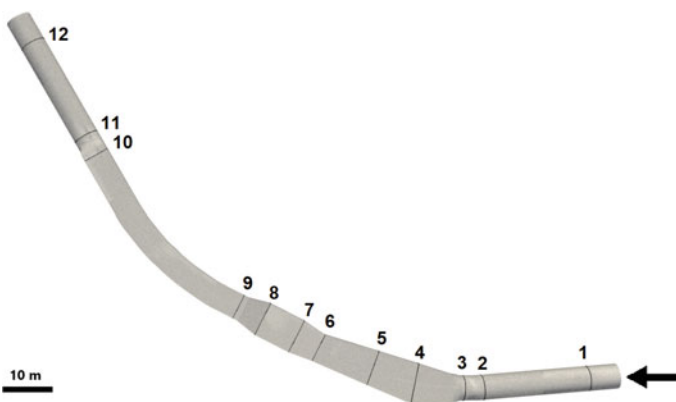


**Fig. 61.5** Positioning of the 12 measurement locations representing changes in hydraulic section

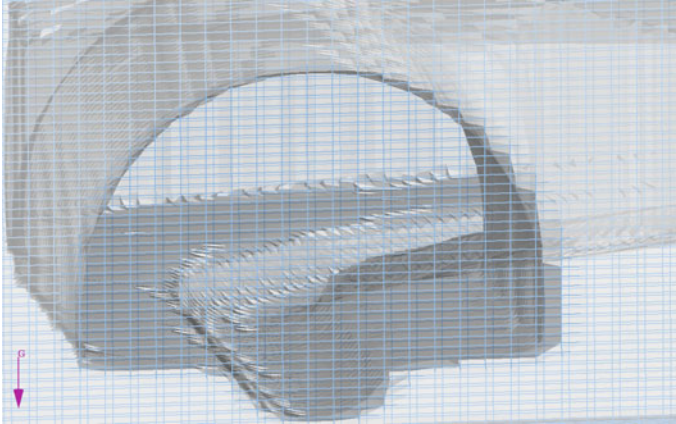


**Fig. 61.6** Visualisation of the Flow-3D mesh with rectangular elements

### 61.3.1.2 Flow-3D

A second 3D numerical model was set up in Flow-3D, which takes into account the gravity and turbulence physics models. The water was modelled at 20° C with a density of 1000 kg/m<sup>3</sup> and a dynamic viscosity of 0.001 kg/m/s. The gravity acceleration was defined to be 9.8 m/s<sup>2</sup>. The k-ε model was chosen as the turbulence model in the Reynolds Averaged Navier Stokes (RANS) equations. Flow-3D numerically solves the continuity and momentum equations using finite-volume approximation.

The flow region was subdivided into a mesh of fixed rectangular cells (30 cm in  $x$  and  $y$ , 10 cm in  $z$ ; Fig. 61.6). With each cell there are associated local average values of all dependent variables. All variables are located at the centers of the cells except for velocities, which are located at cell faces (staggered grid arrangement). Curved obstacles, wall boundaries and other geometric features are embedded in the mesh by defining the fractional face areas and fractional volumes of the cells that are open to flow. The Fractional Area-Volume Obstacle Representation (FAVOR) method used exclusively in Flow-3D eliminates the stair step effect that might otherwise occur with a simple Cartesian grid system by smoothly blocking out fractional portions of grid cell faces and volumes.

A no-slip condition was considered on the solid walls. In the current study and for a sufficiently small  $k_s$  (equivalent sand roughness coefficient) compared to the much larger grid size, this will lead to a wall being treated as a smooth surface.

## 61.3.2 Physical Model

A reduced-scale physical model was built according to Froude similarity with  $\lambda = 20$ . The construction material primarily consisted of PVC (Fig. 61.7). The slope

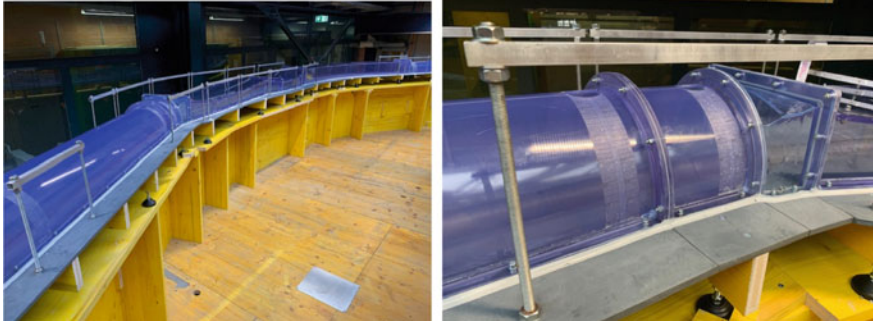


**Fig. 61.7** View of the physical model with the measurement railings on the side looking downstream (left). Measurements of water level were done on the left and right sides by reading off scale bars and in the center with a needle gauge (right)

was fitted by regularly spaced adjustable legs. Flow to the model is supplied by the internal hydraulic circuit of the laboratory. The measurement locations were the same as for the numerical model. Measurement location 2 (refer to Fig. 61.5) was used for the roughness calibration. Only one discharge scenario could be fully tested ( $Q = 40 \text{ m}^3/\text{s}$ ) due to higher water levels than expected. Discharges ranging from  $Q = 2 \text{ m}^3/\text{s}$  to  $Q = 67 \text{ m}^3/\text{s}$  were tested to establish the rating curve. An electric resistance needle gauge was used to measure the time averaged water surface elevation at the center of the sections even with slightly wavy flow conditions.

## 61.4 Results

### 61.4.1 Model Validation

Figure 61.8 presents the results of the numerical model validation, which was carried out at measurement location 2. For all discharges, the 1D HEC-RAS water surface profile is lower than the 3D results, with the difference increasing as discharge increases. The theoretical Strickler analysis predicts a slightly higher normal water depth than the 3D water surface profile for the design discharge, with a difference of 0.12 m (4%). A comparison to the physical model for  $Q = 40 \text{ m}^3/\text{s}$  shows that a higher water level is measured on the physical model compared to the 1D and 3D models, roughly 0.3 m higher.

The rating curves obtained from the 3D Fluent, Flow-3D and 1D HEC-RAS models, as well as experimental data from the physical model and the normal height from the theoretical Strickler analysis are presented in Fig. 61.9. The 1D results indicate slightly lower water levels compared to the physical model and the 3D models. The 1D HEC-RAS simulation of the water line takes into account cross-sectional average minor loss due to the presence of a bend. At low discharges, the

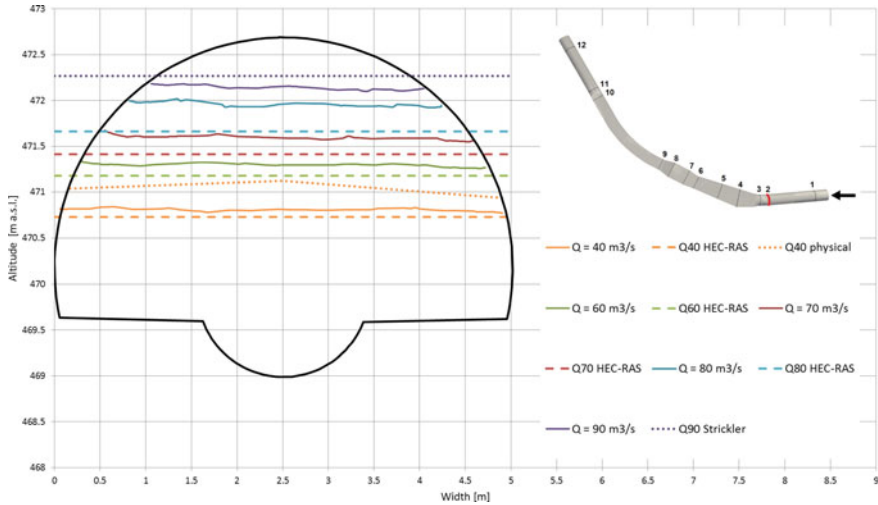


**Fig. 61.8** Validation of the 3D Fluent numerical model for cross-section 2 by comparing to the 1D HEC-RAS results for varying discharges. The design discharge predicted by the 1D model far exceeds the cross-section height, as pressurized flow occurs. In this case, the strickler analysis is provided instead. Comparison to the physical model was only possible for discharge values below some  $70 \text{ m}^3/\text{s}$

physical model coincides with the Strickler analysis, while as discharge increases, so does the deviation from the Strickler analysis. The 3D Fluent results follow closely the theoretical Strickler analysis, while the Flow-3D model estimates a slightly higher water level. The 3D Fluent model predicts a Froude number close to 1 for all discharge scenarios, while the theoretical Strickler analysis and 1D HEC-RAS models predict supercritical flow conditions all along.

It is hypothesized that the water surface elevation prediction from the 3D numerical model has an accuracy of  $\pm$  half the vertical mesh cell size. Flow-3D and Fluent both use the VOF technique, which is based on the idea that in each grid cell the fractional portion  $F$  of the cell volume that is occupied by the fluid is given. The fractional volume  $F$  has a value between 0.0 and 1.0 and the free surface is located in any cell element having an  $F$  value lying between these limits. Thus, the upper limits of the free surface predicted by the two 3D numerical models follow closely the lower limit of the physical model measurements.

### 61.4.2 Water Surface Profiles

The cross-sectional water surface profiles are shown in Fig. 61.10 for cross-section 4. For  $Q = 70, 80$  and  $90 \text{ m}^3/\text{s}$ , the water level touches the ceiling locally at cross-sections 4, 5, 7 and 9. At cross-section 7, the design discharge fills the entire hydraulic

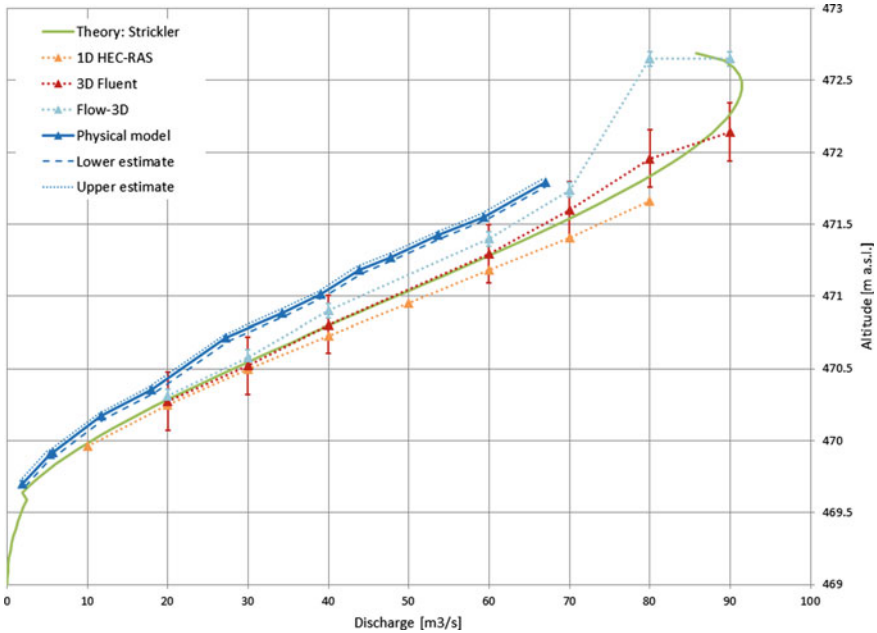


**Fig. 61.9** Rating curves for the theoretical strickler analysis (green, continuous line), 1D HEC-RAS model (orange), 3D Fluent model (red), Flow-3D model (light blue) and physical model (dark blue). The hypothetical water surface elevation accuracy of the two 3D numerical models is given by the error bars and represents half the maximum mesh element size in the  $z$  direction (0.2 m for Fluent and 0.05 m for Flow-3D). The Flow-3D model predicts pressurized flow above a value between 70 and 80  $m^3/s$ , as there is no wall inflation layer close to the ceiling, while the flow in the Fluent model remains at free surface

section. This is also the case at cross-section8 for  $Q \geq 60 m^3/s$ . Therefore, the hydraulic criterion requiring that the water level does not touch the ceiling locally is only fulfilled at cross-section1, 2, 3, 6, 10 and 12 for the design discharge.

The effect of the bend in the geometry is evidenced by the non-horizontal water surface profiles, seen by an inclination towards the outer left. The safety margin and free surface filling ratio hydraulic criteria are only fulfilled for the design discharge at cross-section 1 and 3. At cross-sections 7 and 8, corresponding to the m2 stretch, none of the simulated discharges fulfils these two hydraulic criteria. These results identify the most problematic cross-sections to be along the m2 stretch (cross-sections 7 and 8). The problematic region is not only limited to the m2 stretch, as the pressurized flow taking place at cross-section 8 is likely to explain the high water levels at the next downstream cross-section 9, as this cross-section presents a greater hydraulic section.

The longitudinal profiles of the water surface along the center line of the geometry for five discharge scenarios are given in Fig. 61.11. The five scenarios show similar patterns, with a decrease in water level underneath the m3 stretch due to the local widening of the section. Following this, the water level for  $Q = 40$  and 60

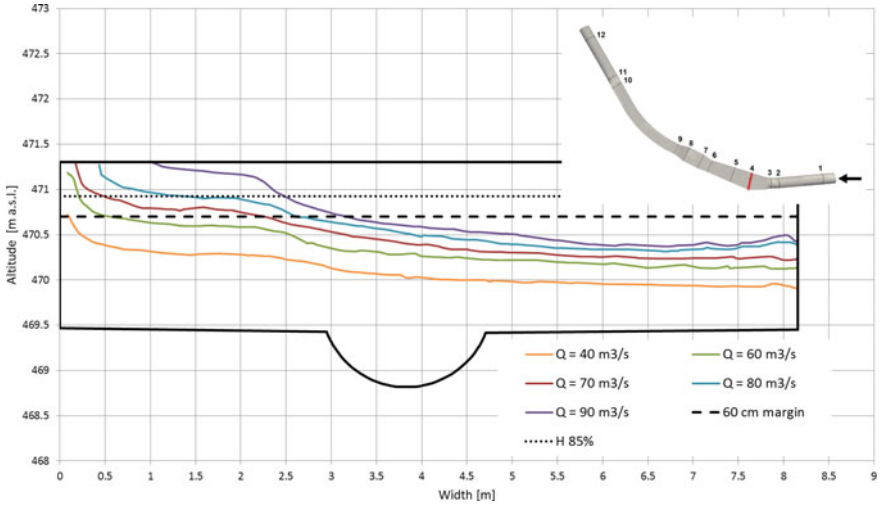


**Fig. 61.10** Water surface profiles from Fluent for cross-section 4 (m3 stretch, view in flow direction) for  $Q = 40 \text{ m}^3/\text{s}$  (orange),  $Q = 60 \text{ m}^3/\text{s}$  (green),  $Q = 70 \text{ m}^3/\text{s}$  (red),  $Q = 80 \text{ m}^3/\text{s}$  (turquoise) and the design discharge  $Q = 90 \text{ m}^3/\text{s}$  (purple). The effect of the non-horizontal water surface due to the bend is clearly visible

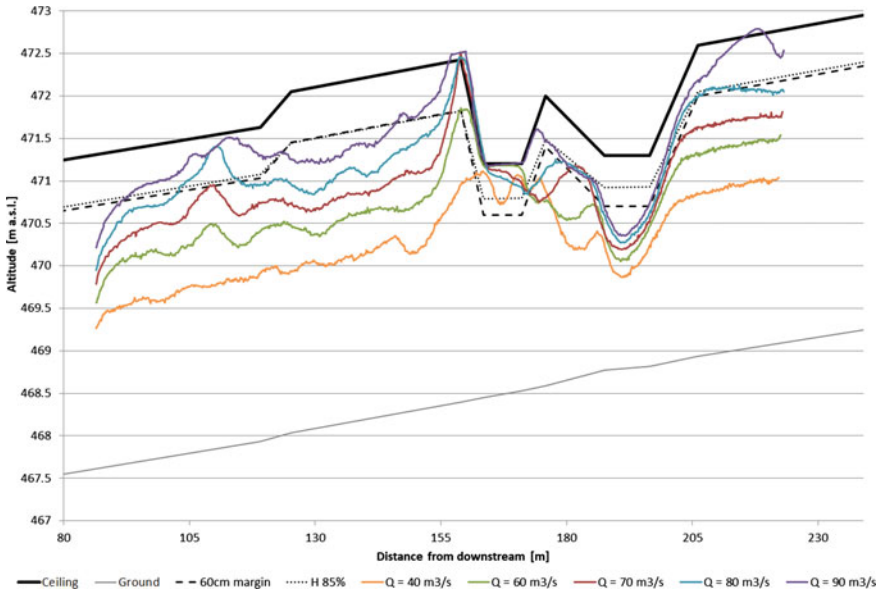


**Fig. 61.11** Longitudinal water surface profile from the Fluent model along the center line of the geometry for five discharge scenarios. The horizontal axis refers to the distance from downstream of the 1D HEC-RAS model, in order to facilitate comparison

$m^3/s$  increases slowly towards the  $m2$  stretch, with the water level for  $Q = 60 m^3/s$  reaching the ceiling of the  $m2$  stretch. In contrast, for  $Q = 70, 80$  and  $90 m^3/s$ , the decrease in water level underneath the  $m3$  stretch is followed by a sharp increase at the transition between the  $m3$  and  $m2$ . This is likely to be a hydraulic jump, which was also evidenced in the 1D HEC-RAS model. Following the  $m2$  stretch, which is characterized by the most limiting ceiling height, the water level increases again for all discharges due to an increase in cross-section height, before slowly levelling off throughout the LEB stretch. Finally, following the transition from the LEB stretch to the historical vaulting, which coincides with a narrowing of the hydraulic section, the water level increases again. The water surface profiles extend well beyond the two hydraulic criteria presented in Fig. 61.10 and the only discharge at which the ceiling is not touched locally is  $Q = 40 m^3/s$ .

The longitudinal water surface profile for the left and right banks based on the 3D numerical model and experimental data from the physical model is given for  $Q = 40 m^3/s$  (Fig. 61.12). The greatest differences in water level between the left and right banks, as well as between the numerical and physical models, are seen underneath the  $m3$  stretch. The numerical and physical models coincide closely for the LEB stretch. Overall, the physical model predicts higher water levels than the numerical model.

Measurements on the physical model all along the model were only possible for  $Q \leq 40 m^3/s$ , except at measurement location 2. The experimental data were added to the

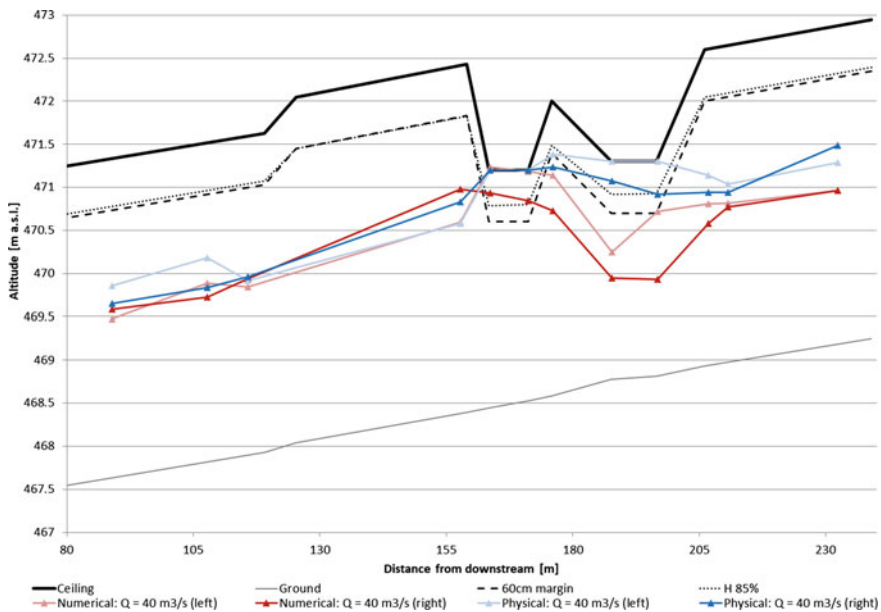


**Fig. 61.12** Longitudinal water surface profiles from the Fluent model for the left and right banks for  $Q = 40 m^3/s$  based on the numerical model (red) and physical model (blue)



**Fig. 61.13** Hydraulic phenomena on the physical model at  $Q = 17.9 \text{ m}^3/\text{s}$  (10 l/s on the model). A shockwave (red outline) on the m3 stretch was formed from left to right (left). The wave is caused by the sharp edge, which corresponds to the bend in the geometry. A hydraulic jump immediately upstream of the lowered m2 stretch was also seen (right)

previous figures for comparison to the numerical model. Photographs of the hydraulic conditions in the physical model are shown in Figs. 61.13 and 61.15. Two hydraulic phenomena were evidenced: a shockwave and hydraulic jump, as the flow is mainly supercritical. A shockwave on the m3 stretch was already visible at low discharges as soon as the flow extended beyond the invert capacity. This was also visible on the 3D numerical model (example from Flow-3D, Fig. 61.14). This shockwave can be explained by the abrupt geometrical transition between two differing hydraulic sections. Specifically, this is caused by the sharp change in flow direction. This shockwave remained present at higher discharges, but at a higher water level and an observed increase in speed of propagation. At low discharges, a hydraulic jump was present immediately upstream of the m2 stretch. This hydraulic jump can be explained by a local change in flow regime from supercritical to subcritical, caused by a reduction in hydraulic section underneath the m2 stretch. Increasing the discharge led to a displacement of the hydraulic jump upstream of the m3 stretch. At  $Q = 28 \text{ m}^3/\text{s}$ , water already began to touch the m2 ceiling locally at the left outer edge, and by  $40 \text{ m}^3/\text{s}$ , the entire hydraulic section of the lowest m2 stretch was filled with water. This causes the water level to rise upstream and downstream of the lowered section as well.



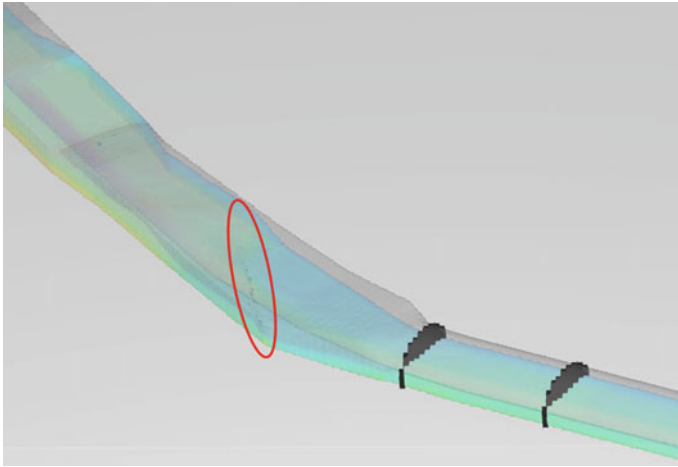


**Fig. 61.14** Shockwave visible on the Flow-3D model (circled in red)

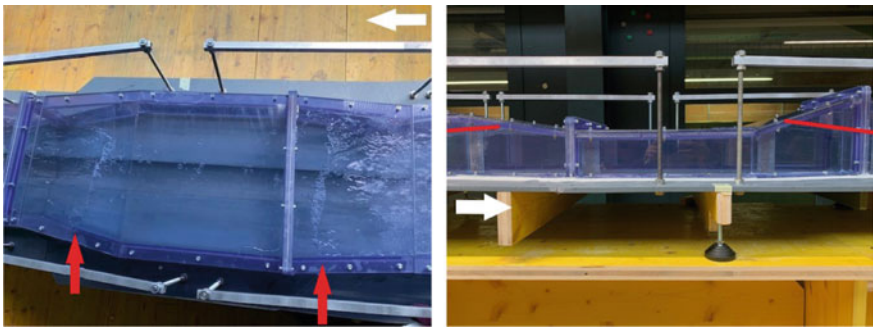


**Fig. 61.15** Hydraulic phenomena on the physical model for  $Q = 40 \text{ m}^3/\text{s}$  (22.4 l/s on the model), with the flow direction indicated by the white arrows. The top view of the m2 stretch, with red arrows indicating the extent over which the flow fills the entire hydraulic section (left). Side view of the m2 stretch (right). The red lines indicate the water level upstream and downstream of the lowered stretch. The flow fills the entire hydraulic section of the lowered section, causing the water level to rise upstream and downstream

## 61.5 Discussion

### 61.5.1 Assessment of the Capacity Limit of the System

The 3D numerical and physical models revealed that the design discharge exceeds the free surface capacity limit of the system. Specifically, at the two cross-sections of the m2 stretch, the design discharge completely fills the hydraulic section, indicating pressurized flow conditions. Even at lower discharges, these two cross-sections do not

allow a locally sufficient freeboard below the ceiling. Specifically, pressurized flow is likely to occur at cross-section 8 for  $Q \geq 60 \text{ m}^3/\text{s}$  and already at  $Q = 40 \text{ m}^3/\text{s}$ , the water level is very close to the ceiling. Results from the 3D Fluent model predict Froude numbers close to 1. Transitional flow behaviour occurs for Froude numbers between 0.7 and 1.5, for which free surface waves, including undular (weak) hydraulic jumps are commonly observed [30]. Model validation revealed that the physical model presents higher water levels for all discharges than both the numerical models. This was also the case for the longitudinal profile, for which the water level reaches the ceiling underneath the m2 stretch. This may suggest that the 3D numerical model underestimates the water level (or that the physical model overestimates it); however, no clear quantifiable indication on the real capacity limit of the system could be given. Another explanation could be a higher roughness of the physical model, but in this case study, the model walls were built with very smooth transparent PVC elements and only the bottom and invert have an artificial roughness according the Froude scaling similitude. However, as the measured and simulated water levels more or less coincide for the lowest tested discharge, this argument can potentially be dismissed.

The three pre-defined hydraulic criteria cannot be met for all measured cross-sections for higher simulated discharges. This suggests that the capacity limit of the system is inferior to  $40 \text{ m}^3/\text{s}$ . This low capacity limit may lead to pressurized flow conditions, causing the flow to rise up to the surface through manholes and gullies in a phenomenon known as geysering [10]. Not only would this be a threat to public safety, but also to the electrical installations of the metro lines at the Flon station.

### 61.5.2 Accuracy

The accuracy of the numerical model is influenced by errors and uncertainties. Errors are primarily caused by numerical approximations, which cannot be eliminated. This is because the Navier–Stokes equations that are solved remain approximations and that convergences criteria requires some limitations. These errors are likely to be insignificant. Uncertainties refer to deficiencies in the model caused by a lack of knowledge [31]. This may be due to uncertainties in the geometry, mesh or boundary conditions. Furthermore, the physics selected to represent the flow may be incorrect or insufficient, such as the turbulence model. The greatest source of uncertainty in this research is likely to be due to the boundary conditions, which would require in-situ data for better parameterization as well as a sensitivity analysis.

The accuracy of the physical model may be influenced due to scale effects, causing differences in behavior between the prototype and model. Given that Froude similarity was applied, scale effects may arise due to Weber (surface tension effects) and Reynolds (viscous effects) numbers. A further source of inaccuracy may originate from the accuracy of the scale bars and the measurements that were taken. The accuracy of the discharge is smaller than  $0.36 \text{ m}^3/\text{s}$  (prototype), and the accuracy of the height is 1 mm (model). Some local waves also occurred, which can affect the local height of the flow. Finally, the roughness may differ from the prototype,

despite attention that was given to reproduce similar roughness according to Froude similarity.

### **61.5.3 Limitations**

The lack of on-site data is considered as the most significant limitation, as no in-situ measurements were available. Therefore, several assumptions had to be made in both the numerical model (e.g. boundary conditions,  $\alpha$  value) and physical model (e.g. surface roughness).

### **61.5.4 Outlook**

The proposed next steps for the m3 engineering project include repeating the hybrid modeling approach on the current vaulting geometry to determine if the current capacity limit meets the requirements of the design discharge. As a next step, the geometry of the m3 stretch should be reviewed.

Future research should aim at obtaining in-situ data to better parameterize the boundary conditions and to calibrate the surface roughness. The influence of the scale effects on the accuracy of the physical model could also be studied.

## **61.6 Conclusions**

The aim of this project was to investigate the choice of the Flon River vaulting reserved space for the construction of the m3 metro line by means of a hybrid approach combining two 3D numerical models and a physical model for a design discharge of 90 m<sup>3</sup>/s. The numerical and physical models revealed that the design discharge exceeds the capacity limit of the system, which is also likely to be the case in the current situation without the planned m3. The modelled capacity limit of the system was evaluated to be below 40 m<sup>3</sup>/s if pressurized flow is to be avoided. Therefore, the proposed geometry for the new m3 metro line cannot be confirmed. The current capacity limit of the system should be evaluated to guide the next steps of the engineering project. Finally, there is great scope for future research to study the limitations and inaccuracies that were identified in this study.

**Acknowledgements** The authors would like to thank everyone involved in the construction of the physical model and for providing data for this research.

## References

1. Buehler R, Pucher J, Gerike R, Goetschi T (2017) Reducing car dependence in the heart of Europe: lessons from Germany Austria, and Switzerland. *Transp Rev* 37:4–28
2. Gerecke M, Hagen O, Bolliger J, Hersperger A, Kienast F, Price B, Pellissier L (2019) Assessing potential landscape service trade-offs driven by urbanization in Switzerland. *Palgrave Commun* 5:13
3. Bosch M, Jaligot R, Chenal J (2020) Spatiotemporal patterns of urbanization in three Swiss urban agglomerations: insights from landscape metrics, growth modes and fractal analysis. *Landscape Ecol* 35:879–891
4. Bourqui P (2018) Rapport n°5466/4001a, Développement des métros m2 et m3 – 1ère étape: Modélisation numérique 1D suite à la modification de la section hydraulique de la galerie souterraine du Flon', Stucky SA. (unpublished project report)
5. Puertas J, Hernandez-Ibanez L, Cea L, Reguerio-Picallo M, Barneche-Naya V, Varela-Garcia F (2020) An augmented reality facility to run hybrid physical-numerical flood models. *Water* 12:13
6. Jarman D, Faram M, Butler D, Tabor G, Stovin V, Burt D, Throp E (2008) Computational fluid dynamics as a tool for urban drainage system analysis: a review of applications and best practice. *11th Int Conf Urban Drainage* 11:10
7. Rubinato M, Lee S, Martins R, Shucksmith J (2018) Surface to sewer flow exchange through circular inlets during urban flood conditions. *J Hydroinfr* 20:564–576
8. Lopes P, Leandro J, Carvalho R, Russo B, Gomez M (2016) Assessment of the ability of avolume of fluid model to reproduce the efficiency of a continuous transverse gully with grate. *J Irrig Drainage Eng* 142:9
9. Djordjevic S, Saul A, Tabor G, Blanksby J, Galambos I, Sabtu N, Sailor G (2013) Ex-perimental and numerical investigation of interactions between above and below ground drainage systems. *Water Sci Technol* 67:535–542
10. Lopes P, Leandro J, Carvalho R, Pascoa P, Martins R (2015) Numerical and experimental investigation of a gully under surcharge conditions. *Urban Water J* 12:468–476
11. Theler D, Reynard E (2006) L'eau en ville Lausanne, 3.1, Atlas hydrologique de la Suisse, Berne
12. Pitteloud A, Duboux C (2001) Lausanne: un lieu, un bourg, une ville. Presses Polytechniques et Universitaires Romandes, Lausanne
13. Szymkiewicz R (2010) Numerical modeling in open channel hydraulics. Springer, Dordrecht
14. Moglen G (2015) Fundamentals of open channel flow. CRC Press, Florida
15. Sturm T (2010) Open channel hydraulics. McGraw-Hill, New York
16. Balkham M, Fosbeary C, Kitchen A, Rickard C (2010) Culvert design and operation guide. CIRIA, London
17. Tullis B (2012) Hydraulic loss coefficients for culverts. *National Coop Highw Res Prog* 734:113
18. Bakhmeteff B (1932) Hydraulics of open channel flow. McGraw-Hill, New York
19. Kessler M, Heller V, Turnbull B (2020) Grain reynolds number scale effects in dry granular slides. *J Geophys Res Earth Surf* 125:19
20. Heller V (2011) Scale effects in physical hydraulic engineering models. *J Hydraul Res* 49:293–306
21. Charbeneau R, Henderson A, Murdock R, Sherman L (2003) Hydraulics of channel expansions leading to low-head culverts. University of Texas, Austin, Center for Transportation Research
22. Sheng W, Alcorn R, Lewis T (2014) Physical modelling of wave energy converters. *Ocean Eng* 84:29–36
23. Hager W, Schleiss A (2009) Constructions hydrauliques: écoulements stationnaires. Presses Polytechniques et Universitaires Romandes, Lausanne
24. Pfister M, Chanson H (2014) Two-phase air-water flows: scale effects in physical modeling. *J Hydrodyn* 26:291–298
25. Hirt C, Nichols B (1981) Volume of fluid (vof) method for dynamics of free boundaries. *J Comput Phys* 19:201–225

26. Duguay J, Lacey R, Gaucher J (2017) A case study of a pool and weir fishway modeled with OpenFOAM and FLOW-3D. *Ecol Eng* 103:31–42
27. Yakhot V, Orszag S (1986) Renormalization group analysis of turbulence. i: basic theory. *J Sci Comput* 1:3–51
28. ANSYS (2013), ANSYS fluent theory guide, vol 15.0. ANSYS, Inc., Canonsburg, PA
29. Samadi-Boroujeni H, Abbasi S, Altaee A, Fattahi-Nafchi R (2020) Numerical and physical modeling of the effect of roughness height on cavitation index in chute spillways. *Int J Civ Eng* 18:539–550
30. Hager W, Gisonni C (2005) Supercritical flow in sewer manholes. *J Hydraul Res* 43:660–667
31. Versteeg H, Malalasekera W (2007) An introduction to computational fluid dynamics: the finite volume method, 2nd edn. Pearson Education Limited, Essex